

Article

The Potential of Multi-Task Learning in CFDST Design: Load-Bearing Capacity Design with Three MTL Models

Zhenyu Wang, Jian Zhou ^{*}  and Kang Peng ^{*}

School of Resources and Safety Engineering, Central South University, Changsha 410083, China; 225512075@csu.edu.cn

^{*} Correspondence: j.zhou@csu.edu.cn (J.Z.); pengkang2020@csu.edu.cn (K.P.)

Abstract: Concrete-filled double steel tubes (CFDSTs) are a load-bearing structure of composite materials. By combining concrete and steel pipes in a nested structure, the performance of the column will be greatly improved. The performance of CFDSTs is closely related to their design. However, existing codes for CFDST design often focus on how to verify the reliability of a design, but specific design parameters cannot be directly provided. As a machine learning technique that can simultaneously learn multiple related tasks, multi-task learning (MTL) has great potential in the structural design of CFDSTs. Based on 227 uniaxial compression cases of CFDSTs collected from the literature, this paper utilized three multi-task models (multi-task Lasso, VSTG, and MLS-SVR) separately to provide multiple parameters for CFDST design. To evaluate the accuracy of models, four statistical indicators were adopted (R^2 , RMSE, RRMSE, and ρ). The experimental results indicated that there was a non-linear relationship among the parameters of CFDSTs. Nevertheless, MLS-SVR was still able to provide an accurate set of design parameters. The coefficient matrices of two linear models, multi-task Lasso and VSTG, revealed the potential connection among CFDST parameters. The latent-task matrix V in VSTG divided the prediction tasks of inner tube diameter, thickness, strength, and concrete strength into three groups. In addition, the limitations of this study and future work are also summarized. This paper provides new ideas for the design of CFDSTs and the study of related codes.

Keywords: axial compression capacity; circular concrete-filled double-skin steel tube column (CFDST); CFDST design; load-bearing capacity; multi-task learning; multi-task Lasso; variable selection and task grouping (VSTG); multi-output LS-SVR (MLS-SVR)



Citation: Wang, Z.; Zhou, J.; Peng, K. The Potential of Multi-Task Learning in CFDST Design: Load-Bearing Capacity Design with Three MTL Models. *Materials* **2024**, *17*, 1994. <https://doi.org/10.3390/ma17091994>

Academic Editors: Piotr Lacki, Janina Adamus, Anna Derlatka, Wojciech Więckowski and Krzysztof Cpałka

Received: 31 March 2024
Revised: 18 April 2024
Accepted: 22 April 2024
Published: 25 April 2024



Copyright: © 2024 by the authors. Licensee MDPI, Basel, Switzerland. This article is an open access article distributed under the terms and conditions of the Creative Commons Attribution (CC BY) license (<https://creativecommons.org/licenses/by/4.0/>).

1. Introduction

Incorporating metal components into concrete is a common approach to reinforce concrete columns [1], and concrete-filled double steel tubes (CFDSTs) have gained considerable traction in recent years. CFDSTs are a load-bearing structure produced by filling concrete between two steel tubes placed concentrically. The unique structure enables CFDST to achieve superior load-bearing capacity while being lighter in weight. Thus, CFDST is widely used in large-scale structures such as super high-rise buildings and highway bridges [2].

Load-bearing capacity [3,4], torsional behavior [2,5], bending resistance [6,7], blast resistance [8–10], and fire resistance [11,12] were assessed in previous studies, wherein CFDSTs with different designs (material combination or structural design) were subjected to various property trials. The experimental results showed that the design of CFDSTs has a significant impact on its properties.

As the most fundamental property of CFDSTs, the load-bearing capacity always needs to be considered. In terms of CFDST design, emphasizing on load-bearing capacity, although some international design codes already exist, such as Eurocode-4 (EC4) [13], ACI [14], and AISC [15], their reliability still remains questionable [16]. Lama et al. [17]

used a non-linear finite element technique to analyze the axial compression capacity of CFDSTs made from a novel material combination. Comparing the above codes with the numerical results, it was found that EC4 and AISC were not suitable for this type of CFDSTs. Hassanein et al. [18] mentioned that the existing design codes of CFDSTs do not take the confinement effect of tubes into account. This is the reason why most models are too conservative in predicting the load-bearing capacity of CFDSTs. To avoid various constraints that make theoretical approaches more complex, machine learning techniques have been adopted, and they have achieved an accuracy far higher than EC4, ACI, and AISC [16]. In other studies, e.g., those of Tran and Kim [19], Wang et al. [4], and Chandramouli et al. [20], the prediction accuracy of the above models (EC4, ACI, and AISC) was also found to be inferior to the recently proposed methods.

However, the core idea of current studies on CFDST design is still to find a mapping from the design parameters to a certain property (e.g., load-bearing capacity) and then to find whether the design is reliable and can be verified via the prediction of this property. In a nutshell, the existing methods are more concerned about “how to verify whether a design is reliable” rather than “how to provide a reliable design directly”. Certainly, this is understandable, as the second issue is a more difficult problem involving multiple outputs.

Figure 1 shows the structure of a conventional CFDST. The main structural parameters include the diameters (D) and thicknesses (t) of the steel tubes, as well as column length (H). Among them, the length of the column is often constant in a specific project. Therefore, the design is usually focused on dimensions and properties of steel tubes, as well as the mechanical properties of concrete. Providing diverse guidance for CFDST design is simultaneously a challenge for the aforementioned methods.

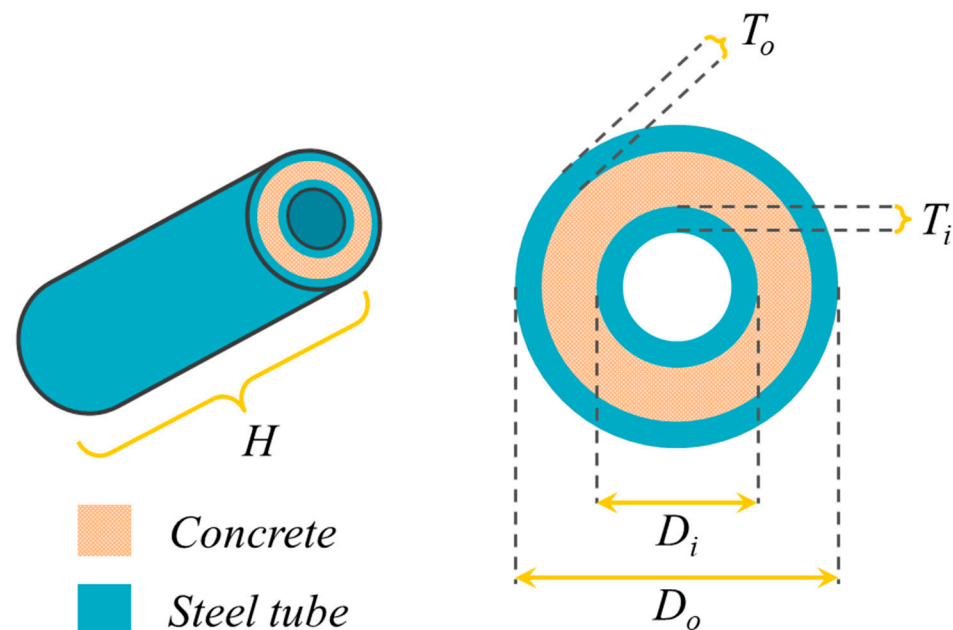


Figure 1. Circular cross-section of a CFDST's structure.

As a branch of machine learning technique, multi-task learning (MTL) has been widely used in fields such as stellar spectra parameterization [21], disease cognitive scores [22], and short-term wind speed prediction [23]. By summarizing the potential correlations of multiple tasks, MTL has shown good performance in solving various multi-output problems. Therefore, using the MTL technique to guide the structural design of CFDSTs is a promising topic. In addition, using the non-linear finite element technique to verify the reliability of CFDST design is often complex. For slender structures and thin-walled structures, the accuracy requirements for modeling and solving vary at different scales [24,25]. The calculation strategy often determines whether the model can quickly converge and accurately predict with limited computational costs on an ordinary computer [26], especially for composite

structures [27] like CFDSTs. With the guidance from MTL, the unnecessary trials and errors can be avoided.

From the perspective of load-bearing capacity, this research attempted to utilize three distinct MTL models for the design of CFDSTs. Based on 227 CFDST cases with circular cross-sections collected from previous literature, the MTL models were trained to provide a reliable set of design parameters. These parameters can serve as references to achieve the desired load-bearing performance. Furthermore, several statistical indicators were used to evaluate the reliability of the provided parameters.

The main content of this paper includes the following sections: Section 2 mainly introduces the models used and explains the model development process; Section 3 presents the hyper-parameter settings and experimental results; Section 4 discusses the findings from the results and lists the limitations of the experiment, as well as discussing future work; Section 5 summarizes the content and significance of this study.

2. Materials and Methods

2.1. Multi-Task Learning Models

In the supervised learning technique, a conventional model can only learn one task during the training phase. For complex problems, they are usually decomposed into several simple problems and then solved separately using single task learning (STL) models. Multi-task learning (MTL) is another kind of supervised learning technique that can achieve inductive transfer among multiple tasks. The information-sharing mechanism enables MTL to update the parameters of all tasks in a single data traversal. More importantly, this mechanism can enhance the generalization ability of each task [28].

The design guidance for CFDST requires a model to provide multiple parameters simultaneously. These output parameters are highly correlated, and each of them can correspond to a task in MTL. This characteristic leads to the compatibility between CFDST design and the MTL technique. This section summarizes the three MTL methods used in this study.

2.1.1. Multi-Task Lasso

Lasso regression is a classic linear regression model proposed by Tibshirani [29]. By introducing the L_1 norm into the loss function of least squares regression, Lasso regression achieved a better generalization ability than conventional linear regression. The loss function of basic Lasso is given as follows:

$$\min_W \frac{1}{2n} \|Y - XW\|_2^2 + \lambda \|W\|_1 \quad (1)$$

where Y is the n -dimensional output vector; X is the matrix of input features; W is the coefficient vector of the linear model; $\|\cdot\|_1$ is the L_1 norm of the vector; $\|\cdot\|_2$ is the L_2 norm of the vector; and λ is the adjustment coefficient.

As the L_1 regularization term $\|W\|_1$ is introduced, sparsity constraint is imposed on the coefficient vector; thereby, the coefficients of unimportant input features will be set to 0. This characteristic also allows Lasso to be widely used in feature selection.

Multi-task Lasso is an extended version of Lasso. It was presented by Obozinski et al. [30] in the problem of multi-task feature selection. Multi-task Lasso assumes that multiple similar tasks have correlated feature selection. Introducing the $L_{2,1}$ norm to replace the L_1 norm in Lasso, this operation leads to information sharing among different tasks during model iteration. The loss function of multi-task Lasso is given as follows:

$$\min_W \frac{1}{2n} \|Y - XW\|_{Fro}^2 + \lambda \|W\|_{2,1} \quad (2)$$

where vectors Y , X , and W become matrix form; $\|\cdot\|_{Fro}$ is the Frobenius norm of matrix; and $\|\cdot\|_{2,1}$ is the $L_{2,1}$ norm of matrix. The mechanism of the $L_{2,1}$ norm in MTL is detailed in the work of Liu et al. [31].

2.1.2. VSTG

Variable selection and task grouping (VSTG) is another MTL model developed based on linear regression [32]. In VSTG, there are two fundamental theories that need to be understood: low-rank hypothesis and structure approach. As prior knowledge, the low rank hypothesis assumes that the information required for multiple similar tasks is always redundant. For example, if two tasks are more related, their selection of input features may be more similar. Therefore, when all tasks iterate simultaneously, the matrix composed of hyper-parameters must be low rank. In MTL, low-rank constraints can encourage models to develop towards low-rank structures. The structure approach means the association between multiple tasks can be represented by a certain structure. Group structure is the most commonly used type, and it is also adopted by VSTG. In VSTG, similar tasks are considered to belong to the same group. Tasks within the same group share more information during the model development phase.

VSTG decomposes the coefficient matrix, W , into two matrices, U and V . Moreover, latent bases are introduced for learning and describing the overlapping structures among different tasks. The matrix decomposition is shown in Figure 2, where the dark cells represent non-zero values, and light cells represent zero values.

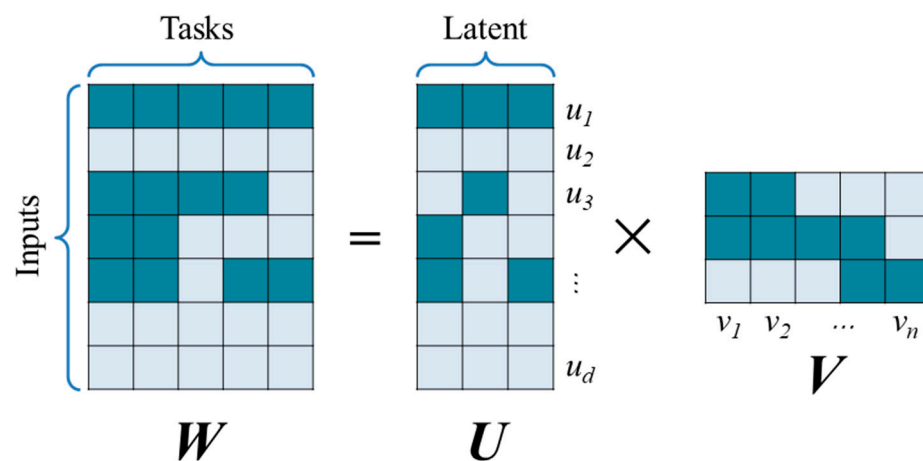


Figure 2. Illustration of matrix decomposition in VSTG.

The matrix U is called the variable-latent matrix, and it records the principal components of input features after the dimensionality reduction operation. The matrix V is called the latent-task matrix, and it records the group structure of tasks. For example, the column vectors v_1 and v_2 are similar in Figure 2, indicating that Task 1 and Task 2 are highly correlated. Thus, these two tasks should belong to the same group. In the training phase, two matrices U and V are updated via ADMM (alternating direction method of multipliers). The loss function of VSTG is given as follows:

$$\begin{aligned} & \min_{U, V} \sum_{i=1}^T \frac{1}{2N_i} \|\vec{y}_i - X_i U \vec{v}_i\|_2^2 \\ & s.t \ \|U\|_1 \leq \varphi_1, \|U\|_{1, \infty} \leq \varphi_2, \\ & \sum_{i=1}^T \left(\|\vec{v}_i\|_k^{sp} \right)^2 \leq \theta \end{aligned} \tag{3}$$

where \vec{v}_i is the i -th column vector in matrix V ; φ_1 , φ_2 , and θ are the parameters of low-rank constraints; $\|\cdot\|_{1, \infty}$ is the $L_{1, \infty}$ norm; and $\|\cdot\|_k^{sp}$ represents the k -support norm.

The constraints in Equation (3) can also exist in the form of regularization terms. Thus, the problem can be transformed into a regularized objective function, as follows:

$$\sum_{i=1}^T \frac{1}{2N_i} \left\| \vec{y}_i - X_i U \vec{v}_i \right\|_2^2 + \lambda_1 \|U\|_1 + \lambda_2 \|U\|_{1,\infty} + \mu \sum_{i=1}^T \left(\left\| \vec{v}_i \right\|_k^{sp} \right)^2 \tag{4}$$

where λ_1 , λ_2 , and μ are regularization parameters.

2.1.3. MLS-SVR

SVR (support vector regression) is a concise and high-performance regression model [33,34]. With the maximum margin mechanism, SVR aims to find the best fitting position for linear models in the feature space. The minority vectors that determine the position of margins are called support vectors. Although SVR uses linear models for regression, it can also be applied to some complex nonlinear problems by adopting soft margin and kernel methods [35–39].

MLS-SVR (multi-output least-squares SVR) is an MTL method developed based on SVR [40]. Unlike the idea of matrix decomposition in VSTG, MLS-SVR believes that the coefficient vectors of different tasks can evolve from an initial coefficient vector. Rewriting a coefficient vector \vec{w}_p into $\vec{w}_o + \vec{u}_p$, the MTL version SVR is dedicated to learning the initial vector \vec{w}_o and evolved component \vec{u}_p from the dataset. Figure 3 shows the illustration of MLS-SVR’s intuition.

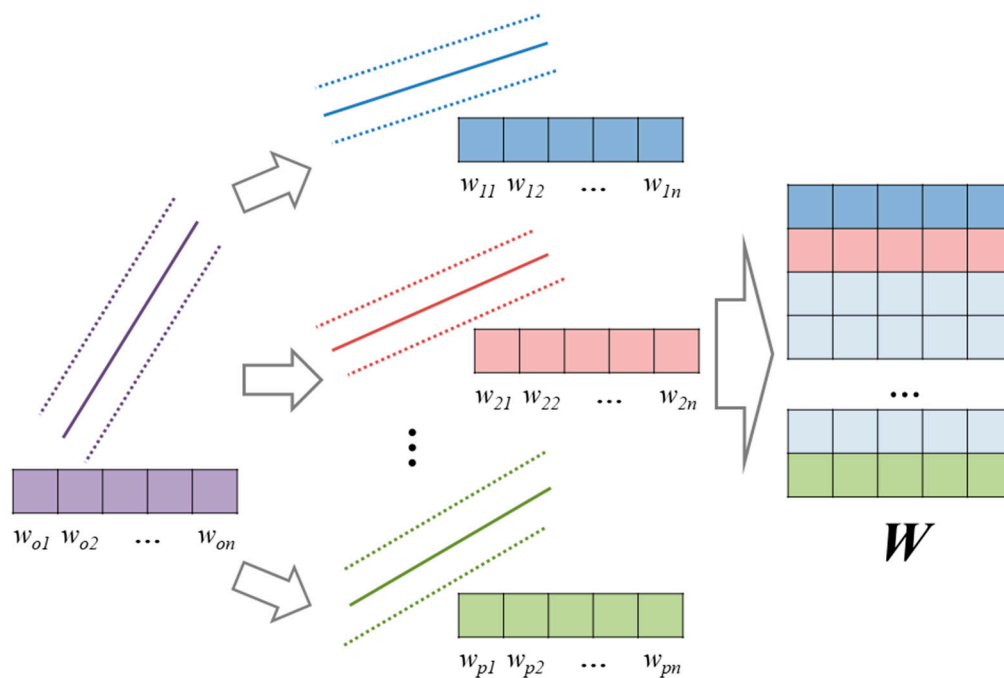


Figure 3. Evolution process of coefficient vectors in MLS-SVR.

In MLS-SVR, the traditional SVR optimization problem has been rewritten into a matrix version, as follows:

$$\begin{aligned} \min_{\vec{w}_o \in \mathbb{R}^p, \Lambda \in \mathbb{R}^p, \vec{b} \in \mathbb{R}^m} & \frac{1}{2} \vec{w}_o^T \vec{w}_o + \frac{1}{2} \frac{\lambda}{m} \text{trace}(\Lambda^T \Lambda) + \beta \frac{1}{2} \text{trace}(\Theta^T \Theta) \\ \text{s.t.} & Y = \Omega^T W + \text{ repmat}(\vec{b}, N, 1) + \Theta \end{aligned} \tag{5}$$

where \vec{w}_o represents the initial coefficient vector; W is the coefficient matrix, wherein elements are \vec{w}_p ; Λ is a matrix composed of \vec{u}_p ; Θ denotes a matrix composed of slack variables from each task; Ω is a matrix used to map input features to higher dimensional

space; \vec{b} is the bias vector; p and m are the dimensions of inputs and outputs, respectively; N is the number of samples in training set; and λ and β are regularization parameters.

2.2. Database

The database used in this study comprises 227 instances of circular cross-section CFDSTs subjected to uniaxial compression [41–60]. These tests were conducted using uniaxial compression testing machines, with sensors installed on the specimens. The data generated from the experiments were automatically collected by the computer.

Table 1 summarizes the 9 parameters required for CFDST design in the database. These parameters are related to the strength of materials (concrete and steel tubes), tube dimensions, and CFDST load-bearing capacity. Additionally, statistical descriptions of the database are given in Table 2. The column length ranging from 230 to 3502 mm included CFDST cases from the laboratory scale to the site scale. In Figure 4, the scatter plot matrix of the database is displayed, and the correlation coefficients between variables are calculated. There, the three parameters, diameter of the outer steel tube, diameter of the inner steel tube, and axial compression capacity of the column were highly correlated. It is worth noting that both D_o and D_i were positively correlated with N_u . However, this makes sense, because a larger column usually means a higher strength.

Table 1. Parameter definitions and descriptions.

| Variables | Descriptions | Note |
|----------------|--|-----------------------|
| H (mm) | Column length | External dimensions |
| D_o (mm) | Diameter of the outer steel tube | |
| D_i (mm) | Diameter of the inner steel tube | Internal dimension |
| t_o (mm) | Thickness of the outer steel tube | Steel tube thickness |
| t_i (mm) | Thickness of the inner steel tube | |
| f_{co} (MPa) | Peak strength of unconfined cylinder ($d \times h = 150 \text{ mm} \times 300 \text{ mm}$) | Concrete strength |
| f_{yo} (MPa) | Yield strength of the outer steel tube | Steel tube strengths |
| f_{yi} (MPa) | Yield strength of the inner steel tube | |
| N_u (kN) | Axial compression capacity | Load-bearing capacity |

Table 2. Statistical description of parameters in the database.

| Parameters | Mean | Median | St. D * | Min | Max |
|----------------|----------|----------|---------|---------|----------|
| H (mm) | 877.830 | 572.000 | 149.429 | 230.000 | 3502.000 |
| D_o (mm) | 220.778 | 165.100 | 32.152 | 74.700 | 603.400 |
| D_i (mm) | 129.618 | 76.000 | 25.742 | 33.500 | 477.000 |
| t_o (mm) | 3.097 | 3.000 | 0.350 | 0.590 | 8.000 |
| t_i (mm) | 2.735 | 2.850 | 0.335 | 0.550 | 8.000 |
| f_{co} (MPa) | 40.813 | 37.500 | 4.094 | 18.700 | 74.700 |
| f_{yo} (MPa) | 362.696 | 350.000 | 20.736 | 177.000 | 549.000 |
| f_{yi} (MPa) | 335.807 | 324.000 | 15.434 | 205.000 | 512.000 |
| N_u (kN) | 2095.051 | 1574.000 | 413.341 | 283.000 | 8950.000 |

* Note: St. D—standard deviation.

2.3. Model Development

Because of various considerations such as materials and economy, the design of CFDSTs is often customized. In practice, a certain type of steel tube or concrete may be prioritized for use, or tubes with a specific dimension may have to be adopted due to special needs (e.g., outer diameter or self-weight of the column). Therefore, the experiments in this study only demonstrated the scenario of providing guidance on inner steel tube and concrete based on the selected outer steel tube.

The inputs and outputs are shown in Table 3. This section demonstrates the development process of the MTL models based on the example scenario. The similar development pattern can be transferred to other situations that have not been demonstrated.

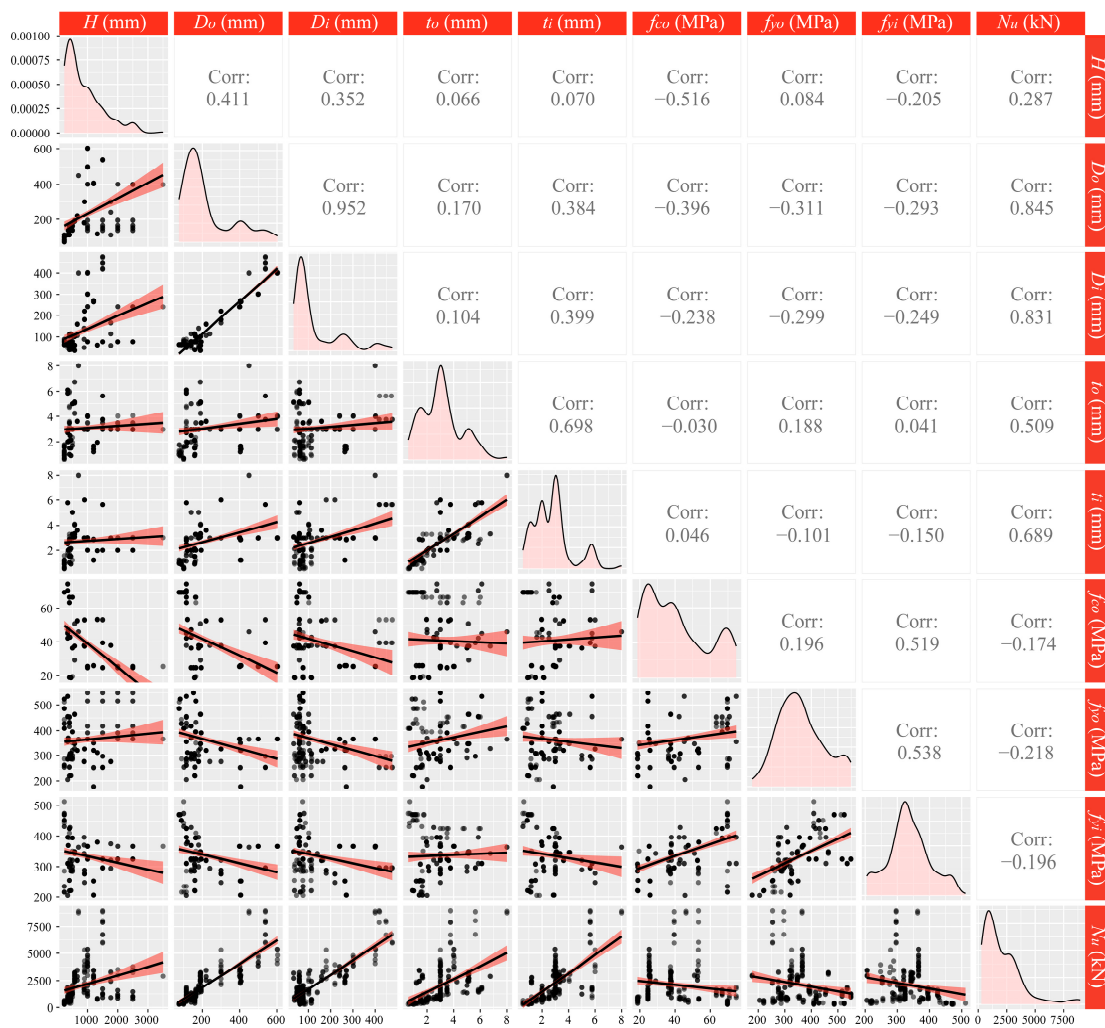


Figure 4. Scatter plot matrix and correlation coefficients of the database (Dots represent the samples, while lines display the distribution trend of dots).

Table 3. The inputs and outputs in the example scenario.

| Inputs | Outputs |
|----------------------------|----------------------------|
| H, D_o, t_o, f_{yo}, N_u | D_i, t_i, f_{yi}, f_{co} |

Different magnitudes of variables may lead to inaccuracy for machine learning models. Especially for MTL, multiple tasks cannot be effectively trained if there is a significant difference in the units. Thus, all variables were normalized into $[-10, 10]$. As the values in the generally used normalization $[-1, 1]$ are too small, $[-10, 10]$ can enable the data-sensitive linear model to learn suitable coefficients successfully.

All samples were allocated to two datasets, namely, the training set (80%) and the testing set (20%) [61]. The training set was used for model development, while the model validation was conducted via a testing set. In supervised learning techniques, there is an assumption that samples and populations follow the same distribution. Therefore, the model development phase requires that the distributions of the training and testing sets are as similar as possible. This partitioning strategy that aims to obtain similar training and testing sets ensures the reliability of model evaluation provided in the testing phase. The distributions of two datasets are shown in Figure 5.

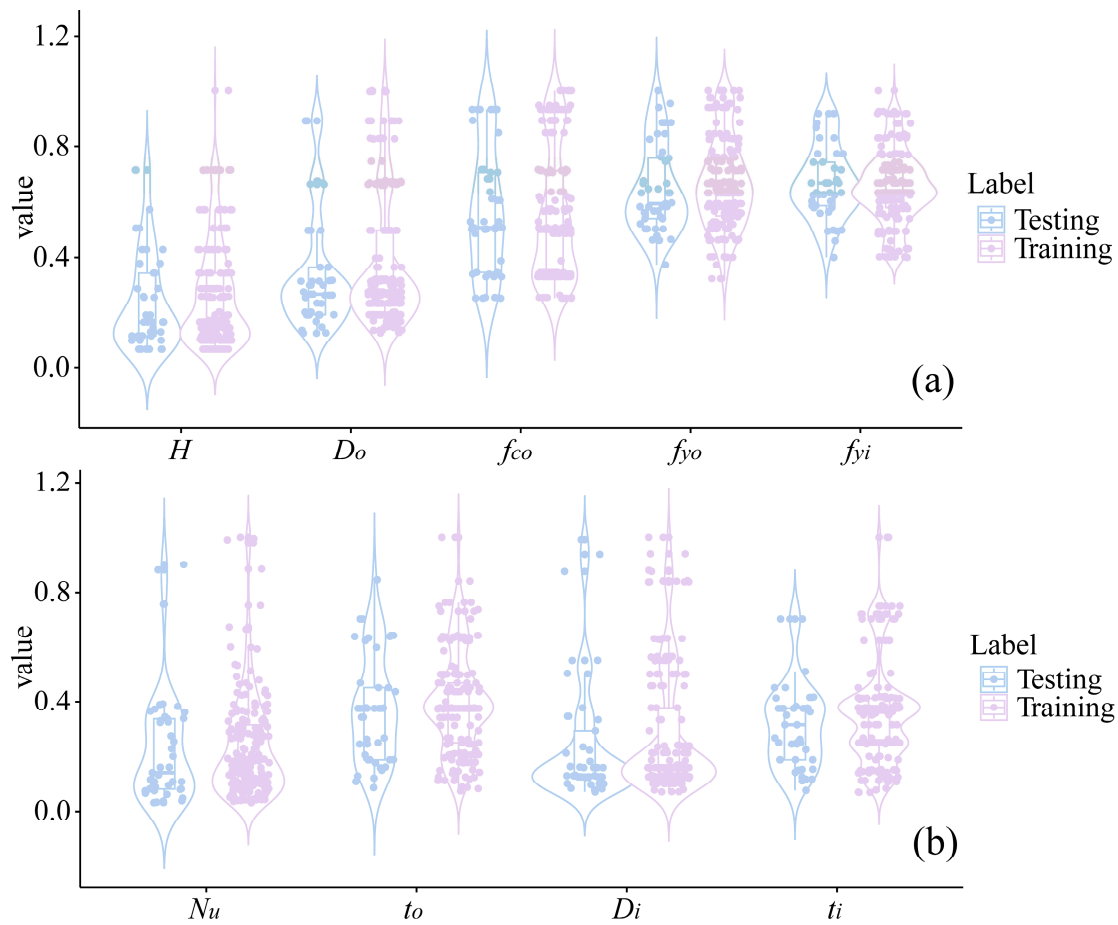


Figure 5. Dataset division and sample distributions in the training and testing sets. (a) division of parameters H , D_o , f_{co} , f_{yo} and f_{yi} ; (b) division of parameters Nu , t_o , D_i and t_i .

Figure 6 shows the entire model development process. Based on the training set, three kinds of MTL models were iterated separately. Subsequently, the testing set was input into these models, and several statistical indicators were adopted to analyze the accuracy of the results.

To evaluate the reliability of the provided parameters, 4 statistical indicators were introduced. Table 4 provides the definitions and expressions of these indicators. The R^2 is generally used to measure the degree of correlation between measurements and predictions [62,63]; RMSE and RRMSE are two indicators used to characterize the error between measurements and predictions [64–69]; and ρ is an indicator that comprehensively considers correlation and error [70,71]. The larger the ρ value, the less accurate the model.

Table 4. Statistical indicators for evaluating the reliability of the provided parameters.

| Statistical Indicators | Expressions |
|--|---|
| Coefficient of determination (R^2) | $\frac{[\sum_{i=1}^N (M_i - \bar{M}_i)(P_i - \bar{P}_i)]^2}{\sum_{i=1}^N (M_i - \bar{M}_i)^2 \sum_{i=1}^N (P_i - \bar{P}_i)^2}$ |
| Root mean square error (RMSE) | $\sqrt{\frac{\sum_{i=1}^N (M_i - P_i)^2}{N}}$ |
| Relative root mean squared error (RRMSE) | $\frac{RMSE}{\bar{P}_i}$ |
| Performance index (ρ) | $\frac{RRMSE}{1 + \sqrt{R^2}}$ |

Note: M—measurement value; P—reference value provided by the model.

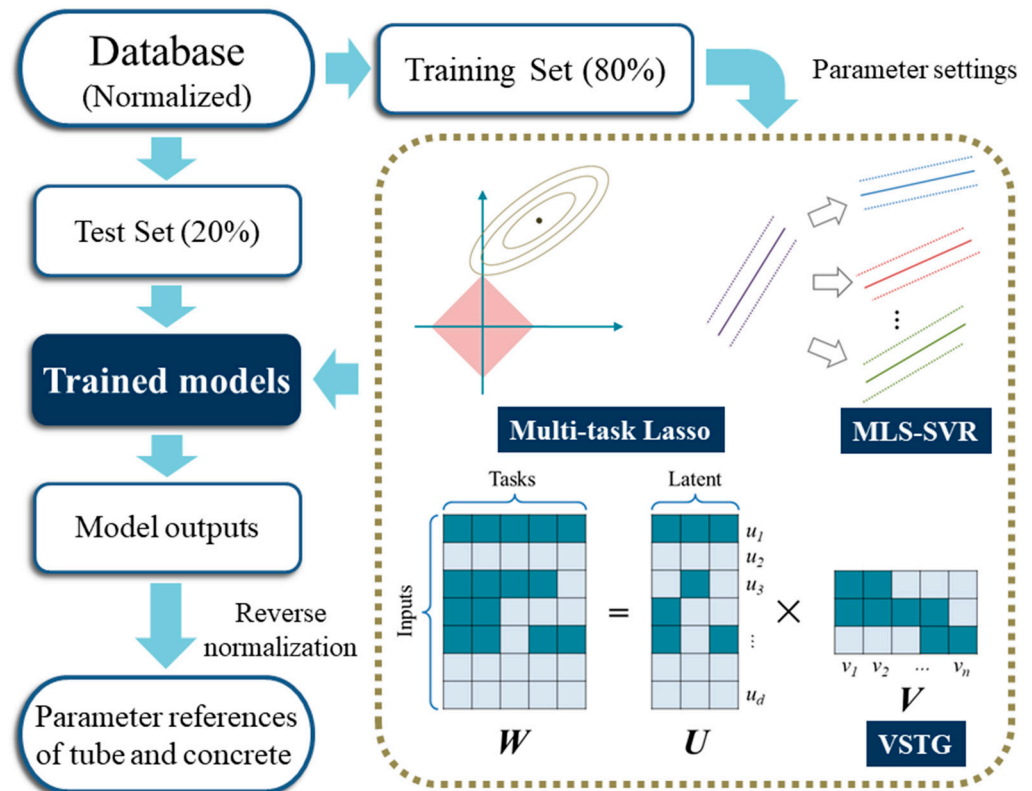


Figure 6. Flowchart of model development.

3. Results

By adjusting and testing, hyper-parameters of three MTL models were obtained separately. With the hyper-parameter settings given in Table 5, three MTL models completed iterations. For each MTL model, the same development process was repeated five times to mitigate errors caused by randomness. All the experimental results are provided in Appendix A.

Table 5. The hyper-parameter settings used for the experiments.

| MTL Models | Hyper-Parameters | Values |
|------------------|--------------------------------------|--------|
| Multi-task Lasso | Regularization parameter λ | 0.091 |
| | Regularization parameter λ_1 | 0.15 |
| | Regularization parameter λ_2 | 0.14 |
| | Regularization parameter μ | 1.25 |
| | k (k -support norm) | 2 |
| VSTG | Number of latent bases M | 3 |
| | Regularization parameter λ | 2.013 |
| MLS-SVR | Regularization parameter β | 33.571 |
| | Kernel function | ERBF |
| | Kernel function parameter σ | 4.493 |

However, the performance of the two linear models on the tasks f_{yi} and f_{co} was not satisfactory enough. Table 6 shows a set of results that was relatively good in experiments of multi-task Lasso (experiment 1), while Table 7 shows an acceptable set of results in VSTG experiments (experiment 1). Compared to strength tasks (f_{yi} and f_{co}), multi-task Lasso and VSTG seemed better at the predictions of dimension tasks (D_i and t_i). As shown in Tables 6 and 7, the R^2 values of strength tasks were at a low level whether on the training set or the testing set. For task f_{yi} , the R^2 was always less than 0.4, and that means the provided f_{yi} was weakly correlated with the actual value. For task f_{co} , two linear models seemed ineffective even on the training set.

Table 6. Statistical evaluation of multi-task Lasso.

| Outputs | Dataset | R ² | RMSE | RRMSE | ρ |
|----------|---------|----------------|--------|-------|--------|
| D_i | Trn | 0.926 | 30.542 | 0.240 | 0.122 |
| | Tst | 0.904 | 34.905 | 0.275 | 0.141 |
| t_i | Trn | 0.648 | 0.866 | 0.312 | 0.173 |
| | Tst | 0.896 | 0.497 | 0.179 | 0.092 |
| f_{yi} | Trn | 0.258 | 56.611 | 0.166 | 0.11 |
| | Tst | 0.457 | 49.811 | 0.146 | 0.087 |
| f_{co} | Trn | 0.382 | 13.915 | 0.306 | 0.189 |
| | Tst | 0.389 | 13.627 | 0.299 | 0.184 |

Note: Trn—training set; Tst—testing set.

Table 7. Statistical evaluation of VSTG.

| Outputs | Dataset | R ² | RMSE | RRMSE | ρ |
|----------|---------|----------------|--------|-------|--------|
| D_i | Trn | 0.922 | 31.210 | 0.245 | 0.125 |
| | Tst | 0.900 | 35.709 | 0.280 | 0.144 |
| t_i | Trn | 0.646 | 0.870 | 0.308 | 0.171 |
| | Tst | 0.898 | 0.513 | 0.182 | 0.093 |
| f_{yi} | Trn | 0.136 | 61.320 | 0.176 | 0.128 |
| | Tst | 0.296 | 56.909 | 0.163 | 0.106 |
| f_{co} | Trn | 0.355 | 14.190 | 0.317 | 0.199 |
| | Tst | 0.390 | 13.473 | 0.301 | 0.186 |

Note: Trn—training set; Tst—testing set.

Unlike the previous two models, MLS-SVR showed quite good performance in all tasks, and the average result of five experiments is displayed in Table 8. From the perspective of task D_i , the RMSE and RRMSE values on the testing set were reduced by 40% compared to multi-task Lasso and VSTG. The RMSE and RRMSE of task t_i also decreased by 20%. Moreover, all the ρ values were below 0.1.

Table 8. Statistical evaluation of MLS-SVR.

| Outputs | Dataset | R ² | RMSE | RRMSE | ρ |
|----------|---------|----------------|--------|-------|--------|
| D_i | Trn | 0.998 | 5.265 | 0.044 | 0.022 |
| | Tst | 0.966 | 20.287 | 0.169 | 0.085 |
| t_i | Trn | 0.973 | 0.239 | 0.093 | 0.047 |
| | Tst | 0.906 | 0.392 | 0.152 | 0.078 |
| f_{yi} | Trn | 0.987 | 7.518 | 0.022 | 0.011 |
| | Tst | 0.965 | 12.633 | 0.037 | 0.019 |
| f_{co} | Trn | 0.975 | 2.754 | 0.064 | 0.032 |
| | Tst | 0.866 | 6.499 | 0.150 | 0.078 |

Note: Trn—training set; Tst—testing set.

Figure 7 displays the scatter plots of predictions provided by MLS-SVR (from experiment 4). Even if there were some outliers in the task t_i (within [2, 4] and [5, 6]) and f_{co} (within [40, 50]) tasks, the distribution of scattering points still showed the accuracy of MLS-SVR in providing parameters for CFDST design. In Figures 8 and 9, the performances of all MTL models in task f_{yi} and f_{co} are compared. It can be noticed that the predictions of the two linear models were conservative in these two unsatisfactory tasks. In other words, the predicted values of two linear models showed the same trend as the actual values increased or decreased, but the degree was not significant.

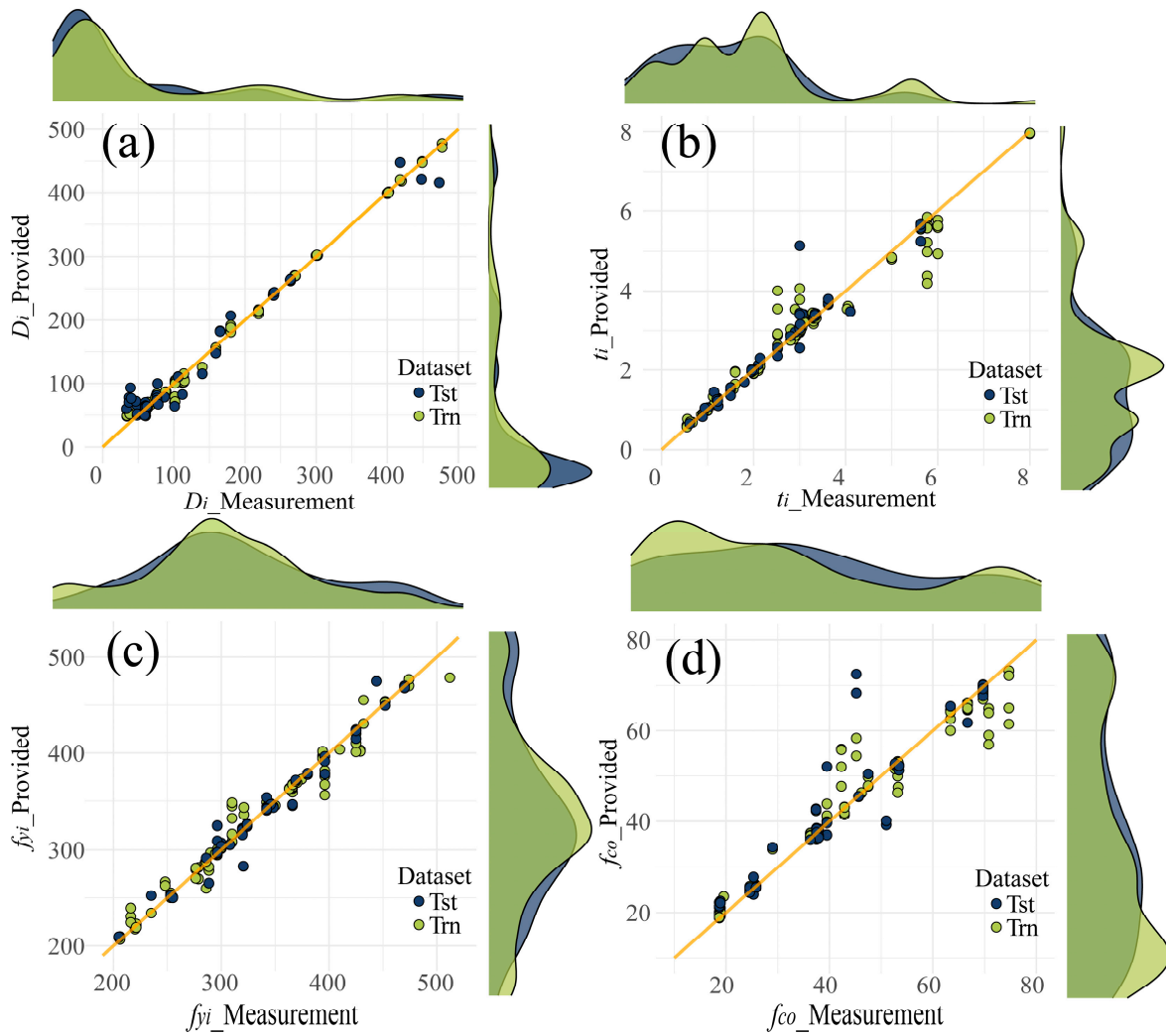


Figure 7. Scatter plots of the provided parameters by MLS-SVR: (a) D_i plot; (b) t_i plot; (c) f_{yi} plot; (d) f_{co} plot.

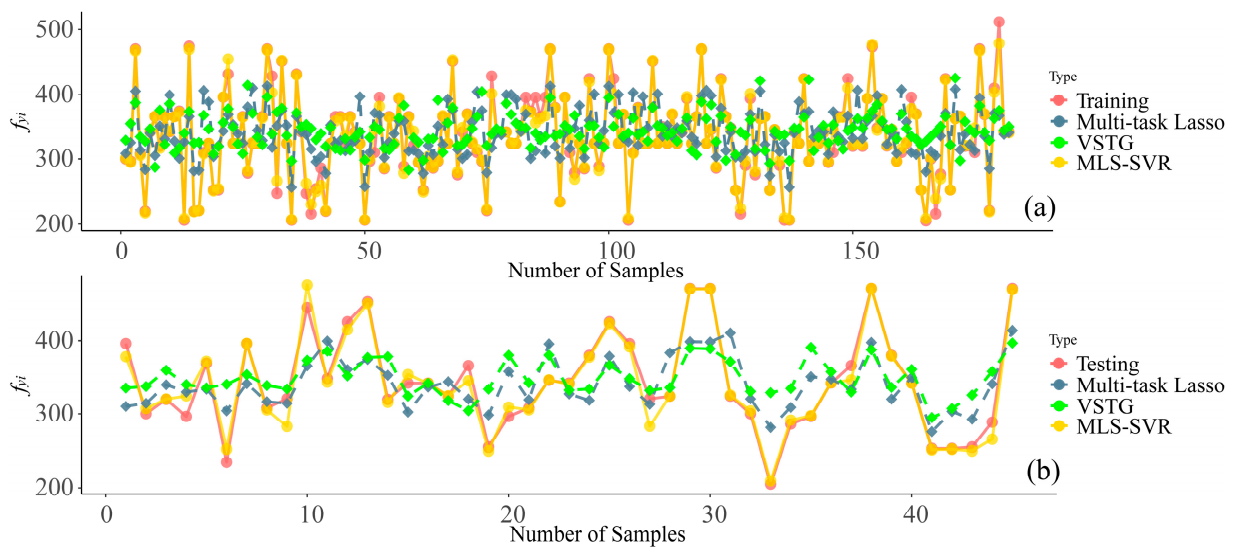


Figure 8. Illustrations of the comparison among MTL provided and the actual values on task f_{yi} : (a) training set; (b) testing set.

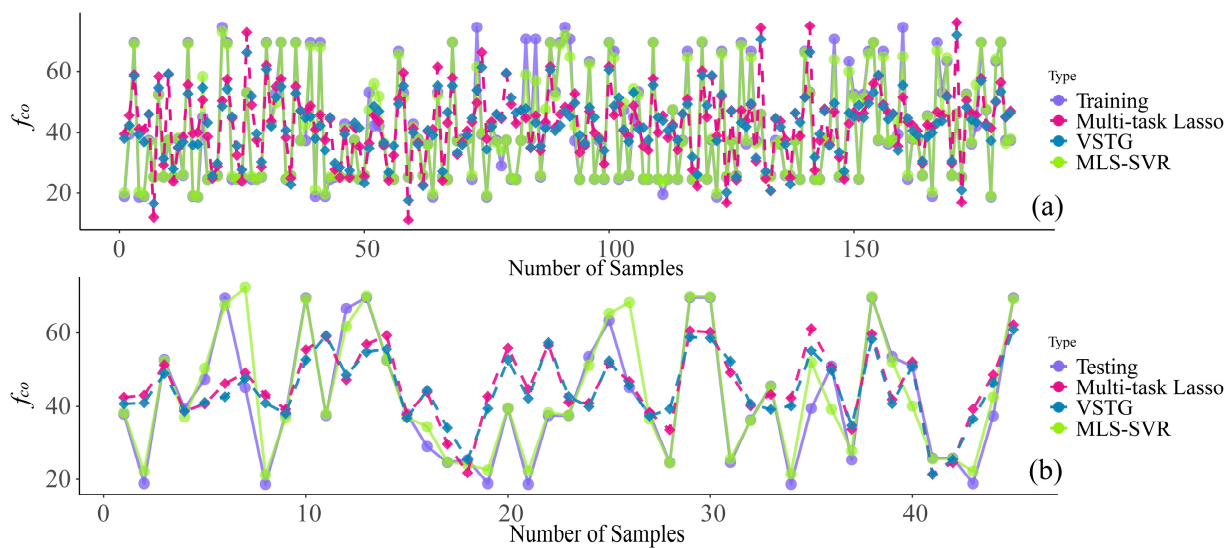


Figure 9. Illustrations of the comparison among MTL provided and actual values on task f_{co} : (a) training set; (b) testing set.

4. Discussion

This section mainly clarifies the problems presented in Section 3, and their causes are also elucidated. Moreover, the feature matrices learned by two linear models are analyzed. Additionally, the limitations and future work are listed at the end of this section.

4.1. Nonlinearity

In the tasks of f_{yi} and f_{co} , linear models were unable to effectively learn the task. Overfitting occurred in both multi-task Lasso and VSTG. Based on this fact, there were two possible causes:

- Cause A: The provided input features did not contain the key information related to the strength tasks. For task f_{yi} and f_{co} , all input features were useless.
- Cause B: There was a certain non-linear relationship between input features and strength tasks. Thereby, linear models were unable to simulate this nonlinearity well.

Cause A can be ruled out, or rather, it cannot be the main issue. This is because the MLS-SVR (with kernel methods for nonlinearity) was able to achieve very accurate predictions in these two tasks, using the same input features.

To further verify cause B, the scatter plots of strength tasks from multi-task Lasso and VSTG are shown in Figures 10 and 11, respectively. In both task f_{yi} and f_{co} , the direction of scatter distribution (blue lines) tended to be horizontal, and that was evidence of nonlinearity between inputs and tasks. For example, if a linear model was used to fit a concave nonlinear function (as shown in Figure 12a), the distribution of scatter would appear in the pattern shown in Figure 12b. With a constant as the boundary, the predicted values within smaller-scale regions were often overestimated, while the predictions within larger-scale regions were often underestimated. Additionally, the more horizontal scatter distribution also indicated the reason why the predictions of two linear models were more conservative in Figures 8 and 9.

4.2. Model Interpretability

Although the two linear models did not excel in all tasks, they had better interpretability. The coefficient matrices (W) obtained from two linear models, as well as variable-latent matrix (U) and latent-task matrix (V) provided by VSTG, all as interpretable components contained the information that revealed the potential correlations among CFDST parameters.

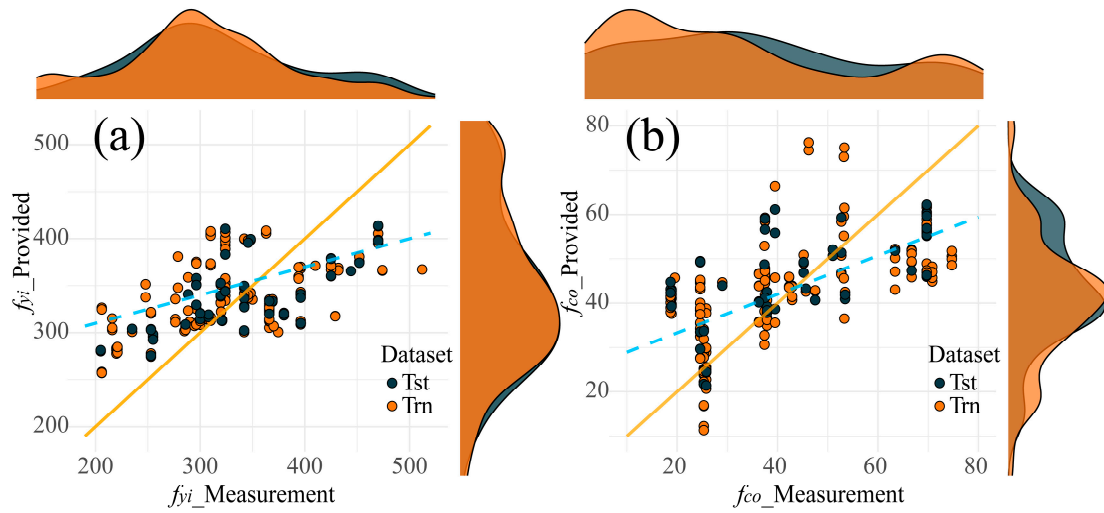


Figure 10. Scatter plots of strength parameters provided by multi-task Lasso: (a) f_{yi} plot; (b) f_{co} plot.

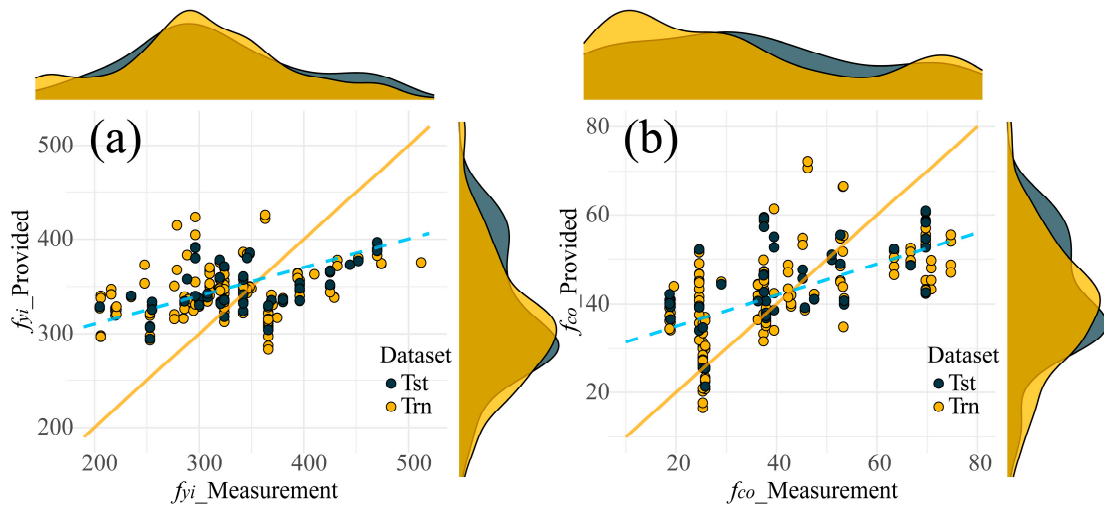


Figure 11. Scatter plots of strength parameters provided by VSTG: (a) f_{yi} plot; (b) f_{co} plot.

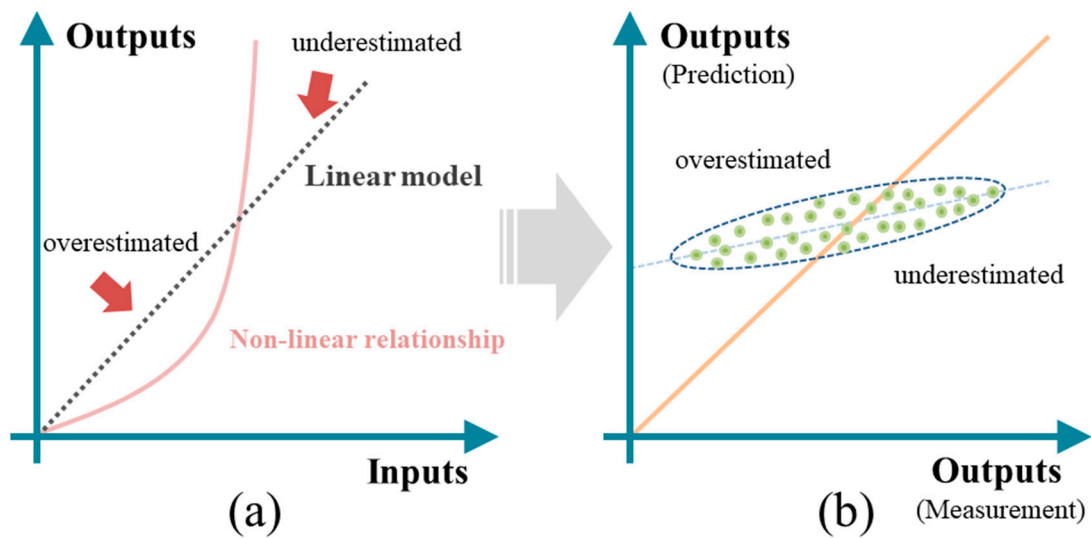


Figure 12. The impact of nonlinearity on linear models: (a) a concave nonlinear function; (b) misguided scatter distribution.

Two coefficient matrices from multi-task Lasso and VSTG are shown in Figure 13. Firstly, the load-bearing capacity (axial compression capacity, N_u) was highly correlated with each output feature, with the strength of concrete contributing the most. Secondly, the contributions of H and f_{yo} to task D_i and task t_i were close to 0. That means the influence of CFDST length and outer tube strength on the inner tube dimension was minimal.

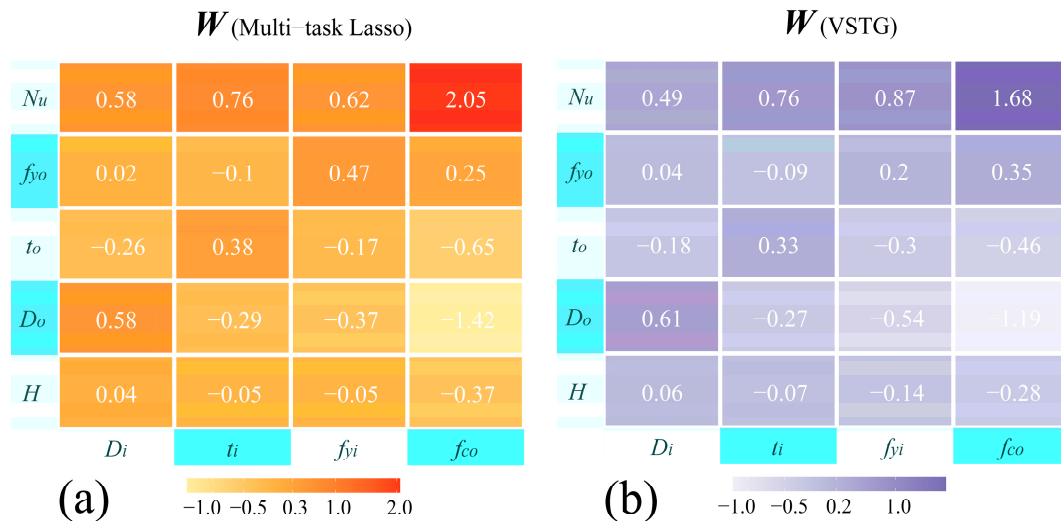


Figure 13. The coefficient matrices obtained from two linear models: (a) W of multi-task Lasso; (b) W of VSTG.

For tasks f_{yi} and f_{co} , there was almost no obvious sparsity in the coefficient vectors (except for the coefficient of H in task f_{yi} in multi-task Lasso). This phenomenon indicated that all inputs were indispensable for both tasks. However, these two models were still unable to fit tasks f_{yi} and f_{co} well. Therefore, it is reasonable to infer that there must have been a lack of certain features, or that potential information had not been fully explored. These inferences were mentioned and answered in Section 4.1. Nevertheless, it is noteworthy that the coefficient vector of task f_{yi} indeed had a relatively stronger sparsity (smaller coefficients) than task f_{co} 's. Perhaps this was the reason why the scatter distribution of task f_{yi} in Figures 10 and 11 was more concentrated, as the dimension of input feature space of task f_{yi} was compressed more effectively.

The variable-latent matrix U and latent-task matrix V from VSTG are shown in Figure 14. The matrix U recorded the mapping from the original input space to the lower dimensional feature space. Figure 14a shows that the input features D_o and f_{yo} were able to be expressed using only two bases in the new feature space, and the projection of feature H on the third base M3 was also almost 0 (Figure 14a). Excess information from the original five-dimensional input space was still able to be fully expressed after being compressed into three-dimensional space. The matrix V is a coefficient matrix used to map the new feature space to the output space. This matrix also stores the group structure among multiple tasks. Seemingly, these tasks can be divided into three groups:

- Group 1 (task D_i): The coefficient of the second base M2 is significantly higher than the other two;
- Group 2 (task t_i): The coefficient of the second base M2 is significantly lower than the other two;
- Group 3 (task f_{yi} and f_{co}): The first base is obviously important, while the values of the other two are almost 0.

This indicates that the diameter and thickness of the inner steel tube are two completely different tasks (their feature selections are opposite), while the strength of the inner steel tube and concrete are very similar tasks.

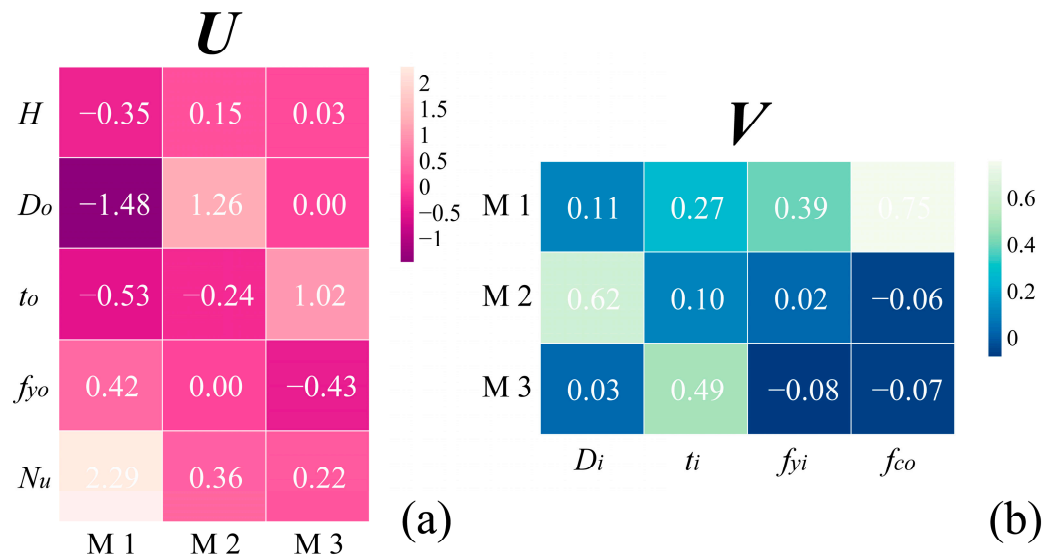


Figure 14. Two matrices provided by VSTG: (a) variable-latent matrix (U); (b) latent-task matrix (V).

4.3. Limitations and Future Work

Although the correlation of models with experimental results demonstrated the potential applications of MTL techniques in guiding CFDST design, there are still many limitations:

- The samples collected in the database were all CFDSTs with circular cross-sections, as this shape is the most conventional. CFDSTs of other shapes may have more parameters, so their design must be more complex.
- MTL is a data-driven approach, and the performance of this technique depends on the quantity and quality of data. Currently, the uniaxial compression cases of CFDSTs are sufficient, while cases of other property trials are still lacking.
- The interpretability of linear models can reveal the potential connection among CFDST parameters. However, this connection is purely mathematical, and the mechanism behind it still remains a mystery.

This study was conducted in a specific condition, and further validations of “whether MTL techniques would be applicable in other situations of CFDST design” will be necessary. As an auxiliary tool, the linear MTL models own good interpretability, and that allows MTL to play a role in the future development of CFDST design codes. In addition, the mechanistic research on CFDSTs (load bearing, failure, etc.) will continue to be crucial. Experiments and cases on the properties of CFDSTs are still lacking.

5. Conclusions

Due to the fact that previous methods can only verify the reliability of a CFDST design and cannot provide direct parameter guidance, this paper proposed using the MTL technique to guide CFDST design. The main works and findings are as follows:

- With 227 uniaxial compression cases of CFDSTs collected from previous literature, three kinds of MTL models were trained to provide multiple parameters for CFDST design. Based on a specific application scenario, the development process of the MTL models was demonstrated.
- During the testing phase, MLS-SVR was able to accurately provide reliable CFDST parameters, while the other two linear models, multi-task Lasso and VSTG, were unable to provide valuable parameters of inner steel tube strength and concrete strength.
- The distribution of scattered points reflected the potential nonlinearity in the task f_{yi} and f_{co} , and the connotation in scatter distribution was discussed in detail. Furthermore, the coefficient matrices of two linear models and the potential group structure among the CFDST parameters were clarified.
- At the end of Section 4, the limitations of the study and future work are also summarized.

In conclusion, the MTL technique has great potential in guiding CFDST design. With a set of directly provided parameters, the workload of engineers in CFDST design will be greatly reduced. Due to the interpretability, linear MTL models can also serve as an analytical tool and assist in the study of the property mechanisms and design standards of CFDSTs.

Author Contributions: Conceptualization, J.Z. and Z.W.; methodology, Z.W.; software, J.Z. and Z.W.; validation, J.Z., Z.W., and K.P.; formal analysis, K.P.; investigation, K.P.; resources, K.P.; data curation, K.P.; writing—original draft preparation, Z.W.; writing—review and editing, J.Z. and K.P.; visualization, J.Z. and Z.W.; supervision, J.Z. and K.P.; project administration, J.Z. and K.P.; funding acquisition, J.Z. and K.P. All authors have read and agreed to the published version of the manuscript.

Funding: This research is partially supported by the National Key Research and Development Program of China—2023 Key Special Project (no. 2023YFC2907400) and the Distinguished Youth Science Foundation of Hunan Province of China (grant nos. 2022JJ10073 and 2023JJ10072).

Institutional Review Board Statement: Not applicable.

Informed Consent Statement: Not applicable.

Data Availability Statement: The data that support the findings of this study are available on request from the corresponding author upon reasonable request.

Conflicts of Interest: The authors declare no conflicts of interest.

Appendix A

Table A1. All experimental results from multi-task Lasso.

| Outputs | Dataset | R ² | RMSE | RRMSE | ρ | |
|------------------|------------------|------------------|-------------|-------------|-------------|-------------|
| D_i | Trn_experiment_1 | 0.925798241 | 30.54154609 | 0.240264793 | 0.12244763 | |
| | Trn_experiment_2 | 0.925798326 | 30.54154601 | 0.240265398 | 0.122447936 | |
| | Trn_experiment_3 | 0.925798412 | 30.54154593 | 0.240266004 | 0.122448242 | |
| | Trn_experiment_4 | 0.925798497 | 30.54154587 | 0.240266661 | 0.122448548 | |
| | Trn_experiment_5 | 0.921823761 | 31.23514035 | 0.24540618 | 0.125199791 | |
| | Trn_mean | 0.925003447 | 30.68026485 | 0.241293797 | 0.122998429 | |
| | Tst_experiment_1 | 0.903852591 | 34.90496 | 0.274591 | 0.140764 | |
| | Tst_experiment_2 | 0.903852949 | 34.90481 | 0.27459 | 0.140764 | |
| | Tst_experiment_3 | 0.903853308 | 34.90466 | 0.27459 | 0.140764 | |
| | Tst_experiment_4 | 0.903853667 | 34.90451 | 0.27459 | 0.140764 | |
| | Tst_experiment_5 | 0.898420822 | 35.83429 | 0.28154 | 0.144539 | |
| | Tst_mean | 0.902766668 | 35.09065 | 0.27598 | 0.141519 | |
| | t_i | Trn_experiment_1 | 0.647650602 | 0.865708461 | 0.312352516 | 0.173070786 |
| | | Trn_experiment_2 | 0.647650541 | 0.86570846 | 0.312353227 | 0.173071183 |
| Trn_experiment_3 | | 0.647650481 | 0.865708459 | 0.312353938 | 0.173071581 | |
| Trn_experiment_4 | | 0.64765042 | 0.865708458 | 0.312354649 | 0.173071978 | |
| Trn_experiment_5 | | 0.642129795 | 0.87523493 | 0.30854615 | 0.171287964 | |
| Trn_mean | | 0.646546368 | 0.867613754 | 0.311592096 | 0.172714698 | |
| Tst_experiment_1 | | 0.895809286 | 0.497392 | 0.179462 | 0.092198 | |
| Tst_experiment_2 | | 0.895808763 | 0.497392 | 0.179462 | 0.092199 | |
| Tst_experiment_3 | | 0.89580824 | 0.497392 | 0.179463 | 0.092199 | |
| Tst_experiment_4 | | 0.895807718 | 0.497392 | 0.179463 | 0.092199 | |
| Tst_experiment_5 | | 0.896319131 | 0.522132 | 0.184067 | 0.094551 | |
| Tst_mean | | 0.895910627 | 0.50234 | 0.180383 | 0.092669 | |

Table A1. Cont.

| Outputs | Dataset | R ² | RMSE | RRMSE | ρ | |
|------------------|------------------|------------------|-------------|-------------|-------------|-------------|
| f_{yi} | Trn_experiment_1 | 0.257824781 | 56.61053299 | 0.166176103 | 0.110213567 | |
| | Trn_experiment_2 | 0.257826623 | 56.61053286 | 0.166176058 | 0.110213404 | |
| | Trn_experiment_3 | 0.257828465 | 56.61053274 | 0.166176012 | 0.110213242 | |
| | Trn_experiment_4 | 0.257830307 | 56.61053264 | 0.166175967 | 0.110213079 | |
| | Trn_experiment_5 | 0.143605727 | 61.05929462 | 0.175032617 | 0.12693149 | |
| | Trn_mean | 0.234983181 | 57.50028517 | 0.167947351 | 0.113556956 | |
| | Tst_experiment_1 | 0.457067241 | 49.81142 | 0.146218 | 0.087239 | |
| | Tst_experiment_2 | 0.457071203 | 49.81112 | 0.146217 | 0.087238 | |
| | Tst_experiment_3 | 0.457075164 | 49.81082 | 0.146216 | 0.087237 | |
| | Tst_experiment_4 | 0.457079126 | 49.81052 | 0.146215 | 0.087237 | |
| | Tst_experiment_5 | 0.309128976 | 56.65101 | 0.162396 | 0.104368 | |
| | Tst_mean | 0.427484342 | 51.17898 | 0.149452 | 0.090664 | |
| | f_{co} | Trn_experiment_1 | 0.382329222 | 13.91468957 | 0.305536581 | 0.188797713 |
| | | Trn_experiment_2 | 0.382332284 | 13.91468953 | 0.305535146 | 0.188796538 |
| | | Trn_experiment_3 | 0.382335346 | 13.91468949 | 0.305533712 | 0.188795363 |
| Trn_experiment_4 | | 0.382338409 | 13.91468947 | 0.305532277 | 0.188794187 | |
| Trn_experiment_5 | | 0.349522654 | 14.25304033 | 0.319577939 | 0.20084028 | |
| Trn_mean | | 0.375771583 | 13.98235968 | 0.308343131 | 0.191204816 | |
| Tst_experiment_1 | | 0.388893448 | 13.62725 | 0.299225 | 0.184296 | |
| Tst_experiment_2 | | 0.388897421 | 13.62727 | 0.299224 | 0.184295 | |
| Tst_experiment_3 | | 0.388901394 | 13.62728 | 0.299223 | 0.184294 | |
| Tst_experiment_4 | | 0.388905367 | 13.62729 | 0.299222 | 0.184293 | |
| Tst_experiment_5 | | 0.383469564 | 13.54646 | 0.303735 | 0.187578 | |
| Tst_mean | | 0.387813439 | 13.61111 | 0.300126 | 0.184951 | |

Table A2. All experimental results from VSTG.

| Outputs | Dataset | R ² | RMSE | RRMSE | ρ | |
|------------------|------------------|------------------|----------|----------|----------|----------|
| D_i | Trn_experiment_1 | 0.922420 | 31.20567 | 0.244677 | 0.124808 | |
| | Trn_experiment_2 | 0.921584 | 31.29855 | 0.245879 | 0.125449 | |
| | Trn_experiment_3 | 0.921693 | 31.27291 | 0.245672 | 0.12534 | |
| | Trn_experiment_4 | 0.921771 | 31.25197 | 0.245519 | 0.125259 | |
| | Trn_experiment_5 | 0.921824 | 31.23514 | 0.245406 | 0.125200 | |
| | Trn_mean | 0.921858 | 31.25285 | 0.245431 | 0.125211 | |
| | Tst_experiment_1 | 0.899683 | 35.70926 | 0.279989 | 0.143693 | |
| | Tst_experiment_2 | 0.898060 | 35.89606 | 0.281997 | 0.144788 | |
| | Tst_experiment_3 | 0.898216 | 35.87198 | 0.281801 | 0.144681 | |
| | Tst_experiment_4 | 0.898334 | 35.85119 | 0.281651 | 0.144599 | |
| | Tst_experiment_5 | 0.898421 | 35.83429 | 0.28154 | 0.144539 | |
| | Tst_mean | 0.898543 | 35.83256 | 0.281396 | 0.14446 | |
| | t_i | Trn_experiment_1 | 0.64555 | 0.870096 | 0.308432 | 0.171022 |
| | | Trn_experiment_2 | 0.642602 | 0.874941 | 0.308653 | 0.171319 |
| | | Trn_experiment_3 | 0.642569 | 0.874921 | 0.308611 | 0.171298 |
| Trn_experiment_4 | | 0.642411 | 0.875007 | 0.308572 | 0.171286 | |
| Trn_experiment_5 | | 0.642130 | 0.875235 | 0.308546 | 0.171288 | |
| Trn_mean | | 0.643052 | 0.874040 | 0.308563 | 0.171243 | |
| Tst_experiment_1 | | 0.897740 | 0.513348 | 0.181972 | 0.093439 | |
| Tst_experiment_2 | | 0.897543 | 0.518708 | 0.182985 | 0.093964 | |
| Tst_experiment_3 | | 0.897429 | 0.51924 | 0.183152 | 0.094053 | |
| Tst_experiment_4 | | 0.896939 | 0.520482 | 0.183548 | 0.094269 | |
| Tst_experiment_5 | | 0.896319 | 0.522132 | 0.184067 | 0.094551 | |
| Tst_mean | | 0.897194 | 0.518782 | 0.183145 | 0.094055 | |

Table A2. Cont.

| Outputs | Dataset | R ² | RMSE | RRMSE | ρ | |
|-----------------------|-----------------------|------------------|----------|----------|----------|----------|
| <i>f_{yi}</i> | Trn_experiment_1 | 0.136017 | 61.32048 | 0.175747 | 0.128395 | |
| | Trn_experiment_2 | 0.142423 | 61.08823 | 0.175156 | 0.127165 | |
| | Trn_experiment_3 | 0.142487 | 61.08705 | 0.175144 | 0.127149 | |
| | Trn_experiment_4 | 0.142957 | 61.07670 | 0.175097 | 0.127057 | |
| | Trn_experiment_5 | 0.143606 | 61.05929 | 0.175033 | 0.126931 | |
| | Trn_mean | 0.141498 | 61.12635 | 0.175235 | 0.127339 | |
| | Tst_experiment_1 | 0.295738 | 56.90902 | 0.163104 | 0.10565 | |
| | Tst_experiment_2 | 0.305408 | 56.78643 | 0.162821 | 0.104868 | |
| | Tst_experiment_3 | 0.306126 | 56.75469 | 0.162723 | 0.104760 | |
| | Tst_experiment_4 | 0.307393 | 56.71041 | 0.162579 | 0.104591 | |
| | Tst_experiment_5 | 0.309129 | 56.65101 | 0.162396 | 0.104368 | |
| | Tst_mean | 0.304759 | 56.76231 | 0.162725 | 0.104847 | |
| | <i>f_{co}</i> | Trn_experiment_1 | 0.355196 | 14.18623 | 0.317429 | 0.198892 |
| | | Trn_experiment_2 | 0.349209 | 14.26040 | 0.319686 | 0.200941 |
| | | Trn_experiment_3 | 0.349363 | 14.25735 | 0.319629 | 0.200889 |
| Trn_experiment_4 | | 0.349489 | 14.25495 | 0.319587 | 0.200850 | |
| Trn_experiment_5 | | 0.349523 | 14.25304 | 0.319578 | 0.200840 | |
| Trn_mean | | 0.350556 | 14.24239 | 0.319182 | 0.200483 | |
| Tst_experiment_1 | | 0.389745 | 13.47301 | 0.301470 | 0.185600 | |
| Tst_experiment_2 | | 0.383357 | 13.55413 | 0.303853 | 0.187661 | |
| Tst_experiment_3 | | 0.383610 | 13.54961 | 0.303762 | 0.187581 | |
| Tst_experiment_4 | | 0.383550 | 13.54818 | 0.303742 | 0.187574 | |
| Tst_experiment_5 | | 0.383470 | 13.54646 | 0.303735 | 0.187578 | |
| Tst_mean | | 0.384746 | 13.53428 | 0.303312 | 0.187199 | |

Table A3. All experimental results from MLS-SVR.

| Outputs | Dataset | R ² | RMSE | RRMSE | ρ | |
|----------------------|----------------------|------------------|----------|----------|----------|----------|
| <i>D_i</i> | Trn_experiment_1 | 0.997956 | 4.950633 | 0.04127 | 0.020645 | |
| | Trn_experiment_2 | 0.998098 | 4.774466 | 0.039817 | 0.019918 | |
| | Trn_experiment_3 | 0.99828 | 4.541585 | 0.037884 | 0.01895 | |
| | Trn_experiment_4 | 0.99679 | 6.21027 | 0.051617 | 0.025829 | |
| | Trn_experiment_5 | 0.997152 | 5.847266 | 0.04864 | 0.024337 | |
| | Trn_mean | 0.997655 | 5.264844 | 0.043846 | 0.021936 | |
| | Tst_experiment_1 | 0.966752 | 20.16726 | 0.168119 | 0.08477 | |
| | Tst_experiment_2 | 0.967065 | 20.06718 | 0.167353 | 0.084377 | |
| | Tst_experiment_3 | 0.96684 | 20.11983 | 0.16783 | 0.084623 | |
| | Tst_experiment_4 | 0.965648 | 20.61851 | 0.171372 | 0.086435 | |
| | Tst_experiment_5 | 0.966064 | 20.46098 | 0.170203 | 0.085836 | |
| | Tst_mean | 0.966474 | 20.28675 | 0.168976 | 0.085208 | |
| | <i>t_i</i> | Trn_experiment_1 | 0.977555 | 0.221349 | 0.086169 | 0.043329 |
| | | Trn_experiment_2 | 0.977566 | 0.221087 | 0.086098 | 0.043293 |
| | | Trn_experiment_3 | 0.980432 | 0.206541 | 0.080415 | 0.040406 |
| Trn_experiment_4 | | 0.963974 | 0.280518 | 0.109174 | 0.055088 | |
| Trn_experiment_5 | | 0.967474 | 0.266504 | 0.103741 | 0.0523 | |
| Trn_mean | | 0.9734 | 0.2392 | 0.093119 | 0.046883 | |
| Tst_experiment_1 | | 0.901291 | 0.402229 | 0.156584 | 0.080326 | |
| Tst_experiment_2 | | 0.901474 | 0.401589 | 0.156391 | 0.080223 | |
| Tst_experiment_3 | | 0.898315 | 0.408791 | 0.159159 | 0.081712 | |
| Tst_experiment_4 | | 0.916494 | 0.368955 | 0.143593 | 0.073361 | |
| Tst_experiment_5 | | 0.912926 | 0.376779 | 0.146668 | 0.075004 | |
| Tst_mean | | 0.9061 | 0.391669 | 0.152479 | 0.078125 | |

Table A3. Cont.

| Outputs | Dataset | R ² | RMSE | RRMSE | ρ |
|------------------|------------------|----------------|----------|----------|----------|
| f_{yi} | Trn_experiment_1 | 0.989376 | 6.803098 | 0.019868 | 0.009961 |
| | Trn_experiment_2 | 0.989653 | 6.711025 | 0.019602 | 0.009826 |
| | Trn_experiment_3 | 0.99114 | 6.20726 | 0.018126 | 0.009083 |
| | Trn_experiment_4 | 0.980407 | 9.245705 | 0.027043 | 0.013588 |
| | Trn_experiment_5 | 0.982968 | 8.620965 | 0.025204 | 0.012656 |
| | Trn_mean | 0.986709 | 7.517611 | 0.021969 | 0.011023 |
| | Tst_experiment_1 | 0.965078 | 12.61071 | 0.036829 | 0.018578 |
| | Tst_experiment_2 | 0.965056 | 12.62965 | 0.036889 | 0.018608 |
| | Tst_experiment_3 | 0.965206 | 12.59698 | 0.036785 | 0.018555 |
| | Tst_experiment_4 | 0.964875 | 12.67916 | 0.037085 | 0.018708 |
| Tst_experiment_5 | 0.964985 | 12.64765 | 0.036977 | 0.018653 | |
| Tst_mean | 0.96504 | 12.63283 | 0.036913 | 0.018621 | |
| f_{co} | Trn_experiment_1 | 0.977615 | 2.637616 | 0.060853 | 0.030599 |
| | Trn_experiment_2 | 0.978519 | 2.583422 | 0.059613 | 0.029968 |
| | Trn_experiment_3 | 0.980582 | 2.456158 | 0.056692 | 0.028485 |
| | Trn_experiment_4 | 0.969402 | 3.094903 | 0.071324 | 0.035939 |
| | Trn_experiment_5 | 0.97116 | 3.000334 | 0.069161 | 0.034833 |
| | Trn_mean | 0.975456 | 2.754487 | 0.063529 | 0.031965 |
| | Tst_experiment_1 | 0.865928 | 6.502839 | 0.15003 | 0.077713 |
| | Tst_experiment_2 | 0.865614 | 6.515199 | 0.15034 | 0.077881 |
| | Tst_experiment_3 | 0.86555 | 6.522601 | 0.150551 | 0.077992 |
| | Tst_experiment_4 | 0.865382 | 6.473133 | 0.149178 | 0.077284 |
| Tst_experiment_5 | 0.865663 | 6.478995 | 0.149347 | 0.077365 | |
| Tst_mean | 0.865628 | 6.498553 | 0.149889 | 0.077647 | |

References

- Chrysanidis, T.; Tegos, I. Axial and transverse strengthening of R/C circular columns: Conventional and new type of steel and hybrid jackets using high-strength mortar. *J. Build. Eng.* **2020**, *30*, 23. [\[CrossRef\]](#)
- Fan, J.-H.; Wang, W.-D.; Shi, Y.-L.; Ji, S.-H. Torsional behaviour of tapered CFDST members with large void ratio. *J. Build. Eng.* **2022**, *52*, 104434. [\[CrossRef\]](#)
- Farahi, M.; Heidarpour, A.; Zhao, X.-L.; Al-Mahaidi, R. Compressive behaviour of concrete-filled double-skin sections consisting of corrugated plates. *Eng. Struct.* **2016**, *111*, 467–477. [\[CrossRef\]](#)
- Wang, G.; Wei, Y.; Zhang, Y.; Liu, L.; Lin, Y. Experimental behavior of concrete-filled double-skin tubular columns with outer galvanized corrugated steel tubes under axial compression. *Eng. Struct.* **2023**, *295*, 116856. [\[CrossRef\]](#)
- Zhang, D.-L.; Jiang, Z.-Q.; Zhao, S.-X.; Lu, G.-B.; Zhou, X.-H.; Wang, Y.-H. Cyclic behavior and ultimate bearing capacity of circular concrete-filled double skin steel tube members subjected to combined compression and torsion. *Thin-Walled Struct.* **2023**, *186*, 110707. [\[CrossRef\]](#)
- Zhao, X.-L.; Grzebieta, R. Strength and ductility of concrete filled double skin (SHS inner and SHS outer) tubes. *Thin-Walled Struct.* **2002**, *40*, 199–213. [\[CrossRef\]](#)
- Uenaka, K.; Kitoh, H.; Sonoda, K. Concrete filled double skin tubular members subjected to bending. *Steel Compos. Struct. Int. J.* **2008**, *8*, 297–312. [\[CrossRef\]](#)
- Fouché, P.; Bruneau, M.; Chiarito, V. Dual-hazard blast and seismic behavior of concrete-filled double-skin steel tubes bridge pier. *J. Struct. Eng.* **2017**, *143*, 04017155. [\[CrossRef\]](#)
- Li, M.; Zong, Z.; Hao, H.; Zhang, X.; Lin, J.; Xie, G. Experimental and numerical study on the behaviour of CFDST columns subjected to close-in blast loading. *Eng. Struct.* **2019**, *185*, 203–220. [\[CrossRef\]](#)
- Li, M.; Zong, Z.; Du, M.; Pan, Y.; Zhang, X. Experimental investigation on the residual axial capacity of close-in blast damaged CFDST columns. *Thin-Walled Struct.* **2021**, *165*, 107976. [\[CrossRef\]](#)
- Lu, H.; Zhao, X.-L.; Han, L.-H. Testing of self-consolidating concrete-filled double skin tubular stub columns exposed to fire. *J. Constr. Steel Res.* **2010**, *66*, 1069–1080. [\[CrossRef\]](#)
- Lu, H.; Zhao, X.-L.; Han, L.-H. FE modelling and fire resistance design of concrete filled double skin tubular columns. *J. Constr. Steel. Res.* **2011**, *67*, 1733–1748. [\[CrossRef\]](#)
- BEng, S.H.; Park, S. EN 1994-Eurocode 4: Design of composite steel and concrete structures. Retrieved May 1994, 10, 2022.
- Code, A. *Building Code Requirements for Structural Concrete (ACI 318-05) and Commentary (ACI 318R-05)*; American Concrete Institute: Farmington Hills, MI, USA, 2005.
- Muir, L.; Duncan, C.J. *The AISC 2010 Specification and the 14th Edition Steel Construction Manual*; Structures Congress 2011: Las Vegas, NV, USA, 2011.

16. Nguyen, T.-A.; Ly, H.-B. *Predicting Axial Compression Capacity of CFDST Columns and Design Optimization Using Advanced Machine Learning Techniques*; Elsevier: Amsterdam, The Netherlands, 2024.
17. Lama, L.; Zhou, F.; Bhatt, N.R. Structural performance and design of stainless steel SHS-concrete-carbon steel CHS double-skin stub columns. *J. Constr. Steel Res.* **2022**, *190*, 107155. [[CrossRef](#)]
18. Hassanein, M.; Silvestre, N.; Yan, X.-F. Confinement-based direct design of circular concrete-filled double-skin normal and high strength steel short columns. *Thin-Walled Struct.* **2023**, *183*, 110446. [[CrossRef](#)]
19. Tran, V.-L.; Kim, S.-E. Efficiency of three advanced data-driven models for predicting axial compression capacity of CFDST columns. *Thin-Walled Struct.* **2020**, *152*, 106744. [[CrossRef](#)]
20. Chandramouli, P.; Jayaseelan, R.; Pandulu, G.; Sathish Kumar, V.; Murali, G.; Vatin, N.I. Estimating the axial compression capacity of concrete-filled double-skin tubular columns with metallic and non-metallic composite materials. *Materials* **2022**, *15*, 3567. [[CrossRef](#)] [[PubMed](#)]
21. Chang, L.; Zhang, P. Application of multi-task lasso regression in the parametrization of stellar spectra. *Chin. Astron. Astrophys.* **2015**, *39*, 319–329.
22. Liu, X.; Goncalves, A.R.; Cao, P.; Zhao, D.; Banerjee, A.; Alzheimer's Disease Neuroimaging Initiative. Modeling Alzheimer's disease cognitive scores using multi-task sparse group lasso. *Comput. Med. Imaging Graph.* **2018**, *66*, 100–114. [[CrossRef](#)]
23. Wang, H.; Wang, J. Short-term wind speed prediction based on feature extraction with Multi-task Lasso and Multilayer Perceptron. *Energy Rep.* **2022**, *8*, 191–199. [[CrossRef](#)]
24. Magisano, D.; Leonetti, L.; Garcea, G. How to improve efficiency and robustness of the Newton method in geometrically non-linear structural problem discretized via displacement-based finite elements. *Comput. Meth. Appl. Mech. Eng.* **2017**, *313*, 986–1005. [[CrossRef](#)]
25. Gonçalves, R.; Ritto-Corrêa, M.; Camotim, D. A large displacement and finite rotation thin-walled beam formulation including cross-section deformation. *Comput. Meth. Appl. Mech. Eng.* **2010**, *199*, 1627–1643. [[CrossRef](#)]
26. Kouhia, R.; Mikkola, M. Some aspects on efficient path-following. *Comput. Struct.* **1999**, *72*, 509–524. [[CrossRef](#)]
27. Otero, F.; Martínez, X.; Oller, S.; Salomón, O. An efficient multi-scale method for non-linear analysis of composite structures. *Compos. Struct.* **2015**, *131*, 707–719. [[CrossRef](#)]
28. Caruana, R. Multitask learning. *Mach. Learn.* **1997**, *28*, 41–75. [[CrossRef](#)]
29. Tibshirani, R. Regression shrinkage and selection via the lasso. *J. R. Stat. Soc. Ser. B Stat. Methodol.* **1996**, *58*, 267–288. [[CrossRef](#)]
30. Obozinski, G.; Taskar, B.; Jordan, M. *Multi-Task Feature Selection*; Technical Report; Statistics Department UC: Berkeley, CA, USA, 2006; Volume 2, p. 2.
31. Liu, J.; Ji, S.; Ye, J. Multi-task feature learning via efficient $l_2, 1$ -norm minimization. *arXiv* **2012**, arXiv:1205.2631 2012.
32. Jeong, J.-Y.; Jun, C.-H. Variable Selection and Task Grouping for Multi-Task Learning. In Proceedings of the 24th ACM SIGKDD International Conference on Knowledge Discovery & Data Mining, London, UK, 19–23 August 2018.
33. Vapnik, V.N.; Vapnik, V. *Statistical Learning Theory*; John Wiley & Sons: New York, NY, USA, 1998.
34. Vapnik, V.N. *The Nature of Statistical Learning Theory*; Springer: New York, NY, USA, 2000.
35. Zhou, J.; Qiu, Y.; Zhu, S.; Armaghani, D.J.; Li, C.; Nguyen, H.; Yagiz, S. Optimization of support vector machine through the use of metaheuristic algorithms in forecasting TBM advance rate. *Eng. Appl. Artif. Intell.* **2021**, *97*, 104015. [[CrossRef](#)]
36. Zhou, J.; Zhu, S.; Qiu, Y.; Armaghani, D.J.; Zhou, A.; Yong, W. Predicting tunnel squeezing using support vector machine optimized by whale optimization algorithm. *Acta Geotech.* **2022**, *17*, 1343–1366. [[CrossRef](#)]
37. García-Gonzalo, E.; Fernández-Muñoz, Z.; Garcia Nieto, P.J.; Bernardo Sánchez, A.; Menéndez Fernández, M. Hard-rock stability analysis for span design in entry-type excavations with learning classifiers. *Materials* **2016**, *9*, 531. [[CrossRef](#)]
38. Huang, J.D.; Xue, J.H. Optimization of SVR functions for flyrock evaluation in mine blasting operations. *Environ. Earth Sci.* **2022**, *81*, 17. [[CrossRef](#)]
39. Qiu, Y.G.; Zhou, J. Short-term rockburst prediction in underground project: Insights from an explainable and interpretable ensemble learning model. *Acta Geotech.* **2023**, *18*, 6655–6685. [[CrossRef](#)]
40. Xu, S.; An, X.; Qiao, X.D.; Zhu, L.J.; Li, L. Multi-output least-squares support vector regression machines. *Pattern Recognit. Lett.* **2013**, *34*, 1078–1084. [[CrossRef](#)]
41. Wei, S.; Mau, S.; Vipulanandan, C.; Mantrala, S. Performance of new sandwich tube under axial loading: Experiment. *J. Struct. Eng.* **1995**, *121*, 1806–1814. [[CrossRef](#)]
42. Elchalakani, M.; Zhao, X.-L.; Grzebieta, R. Tests on concrete filled double-skin (CHS outer and SHS inner) composite short columns under axial compression. *Thin-Walled Struct.* **2002**, *40*, 415–441. [[CrossRef](#)]
43. Tao, Z.; Han, L.-H.; Zhao, X.-L. Behaviour of concrete-filled double skin (CHS inner and CHS outer) steel tubular stub columns and beam-columns. *J. Constr. Steel Res.* **2004**, *60*, 1129–1158. [[CrossRef](#)]
44. Zhao, X.-L.; Tong, L.-W.; Wang, X.-Y. CFDST stub columns subjected to large deformation axial loading. *Eng. Struct.* **2010**, *32*, 692–703. [[CrossRef](#)]
45. Uenaka, K.; Kitoh, H.; Sonoda, K. Concrete filled double skin circular stub columns under compression. *Thin-Walled Struct.* **2010**, *48*, 19–24. [[CrossRef](#)]
46. Chen, J.Y.; Hai, Y. Research on bearing capacity of short concrete filled double skin steel tubes columns under axial compression. *Adv. Mater. Res.* **2011**, *168*, 2154–2157. [[CrossRef](#)]

47. Han, L.-H.; Li, Y.-J.; Liao, F.-Y. Concrete-filled double skin steel tubular (CFDST) columns subjected to long-term sustained loading. *Thin-Walled Struct.* **2011**, *49*, 1534–1543. [[CrossRef](#)]
48. Han, L.-H.; Ren, Q.-X.; Li, W. Tests on stub stainless steel–concrete–carbon steel double-skin tubular (DST) columns. *J. Constr. Steel Res.* **2011**, *67*, 437–452. [[CrossRef](#)]
49. Essopjee, Y.; Dundu, M. Performance of concrete-filled double-skin circular tubes in compression. *Compos. Struct.* **2015**, *133*, 1276–1283. [[CrossRef](#)]
50. Wang, J.; Liu, W.; Zhou, D.; Zhu, L.; Fang, H. Mechanical behaviour of concrete filled double skin steel tubular stub columns confined by FRP under axial compression. *Steel Compos. Struct.* **2014**, *17*, 431–452. [[CrossRef](#)]
51. Chen, J.; Ni, Y.-Y.; Jin, W.-L. Column tests of dodecagonal section double skin concrete-filled steel tubes. *Thin-Walled Struct.* **2015**, *88*, 28–40. [[CrossRef](#)]
52. Duan, Z.K.; Wang, R. Research of the stainless steel-concrete-carbon steel circular concrete-filled double skin steel tubes under axial compression. *Adv. Mater. Res.* **2015**, *1065*, 1349–1353. [[CrossRef](#)]
53. Li, W.; Wang, D.; Han, L.-H. Behaviour of grout-filled double skin steel tubes under compression and bending: Experiments. *Thin-Walled Struct.* **2017**, *116*, 307–319. [[CrossRef](#)]
54. Ekmekyapar, T.; Hasan, H.G. The influence of the inner steel tube on the compression behaviour of the concrete filled double skin steel tube (CFDST) columns. *Mar. Struct.* **2019**, *66*, 197–212. [[CrossRef](#)]
55. Ekmekyapar, T.; Alwan, O.H.; Hasan, H.G.; Shehab, B.A.; Al-Eliwi, B.J. Comparison of classical, double skin and double section CFST stub columns: Experiments and design formulations. *J. Constr. Steel Res.* **2019**, *155*, 192–204. [[CrossRef](#)]
56. Fang, Y.; Wang, Y.; Hou, C.; Lu, B. CFDST stub columns with galvanized corrugated steel tubes: Concept and axial behaviour. *Thin-Walled Struct.* **2020**, *157*, 107116. [[CrossRef](#)]
57. Yan, X.-F.; Zhao, Y.-G. Compressive strength of axially loaded circular concrete-filled double-skin steel tubular short columns. *J. Constr. Steel Res.* **2020**, *170*, 106114. [[CrossRef](#)]
58. Su, R.; Li, X.; Zhong, T.; Zhou, T. *Axial Behavior of Novel CFDST Columns with Outer Welded Corrugated Steel Tubes*; Elsevier: Amsterdam, The Netherlands, 2021.
59. Yang, Y.-F.; Fu, F.; Bie, X.-M.; Dai, X.-H. Axial compressive behaviour of CFDST stub columns with large void ratio. *J. Constr. Steel Res.* **2021**, *186*, 106892. [[CrossRef](#)]
60. Tiwary, A.K. Experimental investigation into mild steel circular concrete-filled double skin steel tube columns. *J. Constr. Steel Res.* **2022**, *198*, 107527. [[CrossRef](#)]
61. Qiu, Y.G.; Zhou, J. Short-Term Rockburst Damage Assessment in Burst-Prone Mines: An Explainable XGBOOST Hybrid Model with SCSO Algorithm. *Rock Mech. Rock Eng.* **2023**, *56*, 8745–8770. [[CrossRef](#)]
62. Zhou, J.; Shi, X.Z.; Du, K.; Qiu, X.Y.; Li, X.B.; Mitri, H.S. Feasibility of Random-Forest Approach for Prediction of Ground Settlements Induced by the Construction of a Shield-Driven Tunnel. *Int. J. Geomech.* **2017**, *17*, 12. [[CrossRef](#)]
63. Zhou, J.; Li, E.M.; Wei, H.X.; Li, C.Q.; Qiao, Q.Q.; Armaghani, D.J. Random Forests and Cubist Algorithms for Predicting Shear Strengths of Rockfill Materials. *Appl. Sci.-Basel* **2019**, *9*, 16. [[CrossRef](#)]
64. Wan, L.; Tang, Z.; Zhang, J.; Chen, S.; Zhou, W.; Cen, H. Upscaling from leaf to canopy: Improved spectral indices for leaf biochemical traits estimation by minimizing the difference between leaf adaxial and abaxial surfaces. *Field Crop. Res.* **2021**, *274*, 108330. [[CrossRef](#)]
65. Yang, P.; Li, C.; Qiu, Y.; Huang, S.; Zhou, J. Metaheuristic optimization of random forest for predicting punch shear strength of FRP-reinforced concrete beams. *Materials* **2023**, *16*, 4034. [[CrossRef](#)] [[PubMed](#)]
66. Nguyen, H.; Bui, X.N.; Topal, E.; Zhou, J.; Choi, Y.; Zhang, W. (Eds.) *Applications of Artificial Intelligence in Mining and Geotechnical Engineering*; Elsevier: Amsterdam, The Netherlands, 2023.
67. Zhang, X.; Yao, J.; Wu, Y.; Liu, X.; Wang, C.; Liu, H. A Method for Predicting the Creep Rupture Life of Small-Sample Materials Based on Parametric Models and Machine Learning Models. *Materials* **2023**, *16*, 6804. [[CrossRef](#)] [[PubMed](#)]
68. Zhou, J.; Chen, Y.X.; Li, C.Q.; Qiu, Y.G.; Huang, S.; Tao, M. Machine learning models to predict the tunnel wall convergence. *Transp. Geotech.* **2023**, *41*, 15. [[CrossRef](#)]
69. Li, C.; Mei, X.; Dias, D.; Cui, Z.; Zhou, J. Compressive strength prediction of rice husk ash concrete using a hybrid artificial neural network model. *Materials* **2023**, *16*, 3135. [[CrossRef](#)]
70. Gandomi, A.; Roke, D. *Intelligent Formulation of Structural Engineering Systems*; Massachusetts Institute of Technology: Cambridge, MA, USA, 2013.
71. Zhang, W.; Goh, A.T. Multivariate adaptive regression splines and neural network models for prediction of pile drivability. *Geosci. Front.* **2016**, *7*, 45–52. [[CrossRef](#)]

Disclaimer/Publisher’s Note: The statements, opinions and data contained in all publications are solely those of the individual author(s) and contributor(s) and not of MDPI and/or the editor(s). MDPI and/or the editor(s) disclaim responsibility for any injury to people or property resulting from any ideas, methods, instructions or products referred to in the content.